ELSEVIER

Journal of Fluids and Structures 18 (2003) 573–593

JOURNAL OF FLUIDS AND STRUCTURES

www.elsevier.nl/locate/jnlabr/yjfls

Investigation of the nonlinear behaviour of damping controlled fluidelastic instability in a normal triangular tube array

C. Meskell*, J.A. Fitzpatrick

Department of Mechanical Engineering, Trinity College, Parsons Building, College Green, Dublin 2, Ireland

Received 14 November 2000; accepted 8 August 2003

Abstract

The fluidelastic behaviour of two normal triangular tube arrays subject to cross flow have been tested. A novel feature of the test facility is an electromagnetic device which has been used to control the system damping and to provide additional excitation. A linearized model of the fluid force is identified for both arrays and it is shown that nonlinear effects are more significant in the denser array. An empirical nonlinear model is proposed for this array and the associated parameters are quantified directly from free response data using the force state mapping technique. Although, the predicted critical velocity is accurately predicted, the limit cycle amplitude is systematically over estimated. Nonetheless, the resulting model shows good qualitative agreement with experimentally determined system behaviour.

1. Introduction

It is well known that a single flexible cylinder in a rigid tube bundle subject to cross flow may experience large amplitude self-excited vibration referred to as fluidelastic instability (FEI). In a heat exchanger this potentially catastrophic phenomenon can cause total failure of a unit within a few hundred hours of operation, as detailed by Paidoussis (1979). A less severe but equally important consequence is the increased fretting wear caused by the tubes impacting with baffles. The subject of fluidelastic instability in tube arrays has been reviewed in some detail by, for example, Price (1995) and Weaver and Fitzpatrick (1988).

Considerable progress has been made towards reliable linear models, both theoretical and semi-empirical, which can predict the critical velocity at which fluidelastic instability occurs. However, the relationship between the dynamic fluid force and the tube motion is inherently nonlinear as the tube vibration is often self-limiting at post-stable flow velocities. Price and Valerio (1990) and Rzentkowski and Lever (1992) have extended linear models to include nonlinear effects, with limited success. Linear fluid force models have also been used in conjunction with nonlinear structural models to investigate tube impacting on baffles (e.g., Paidoussis and Li, 1992). While it is true that structural nonlinearities, such as impacting, will be more significant, Price (1995) noted that a nonlinear fluid force model is still desirable since it will determine the energy available in the system at impact.

This paper presents an experimental study in two normal triangular tube arrays. The necessity of a nonlinear model is explored by first considering a linearized empirical model based on large amplitude motion. An empirical nonlinear fluid force model is then proposed for one of the arrays, and the parameters of the model are quantified using an inverse method, the force state mapping technique. Although previous studies (e.g., Tanaka and Takahara, 1981;

*Corresponding author.
E-mail address: cmeskell@tcd.ie (C. Meskell).

0889-9746/$ - see front matter © 2003 Published by Elsevier Ltd.
doi:10.1016/j.jfluidstructs.2003.08.013

Nomenclature

A	limit cycle amplitude
A_i, B_i, C_i, D_i	coefficients of polynomial curve fit
c_{em}	additional damping from EMS
c_f	linear fluid damping
c_s	linear structural damping
d	tube diameter
E	fluidelastic force
f_n	natural frequency (Hz)
F	restoring force
G_{em}	EMS constant
k_f	linear fluid stiffness
k_s	linear structural stiffness
m_f	fluid added mass
m_s	modal mass of the structural
P	array pitch
R	circuit resistance
T	turbulent excitation force
U	free-stream fluid velocity
U_c	critical free-stream velocity
V_r	reduced gap velocity
W	work
y	tube displacement
α_{1-5}	linearized response parameters
β	cubic fluid damping
δ	logarithmic decrement
δ_r	mass damping parameter
ζ	effective damping ratio
η	cubic fluid stiffness
ω	natural frequency (rad/s)

Chen et al., 1994) have successfully identified linearized parameters for the fluidelastic forces by directly measuring the forces acting on the vibrating tube, these approaches are not readily applicable in this study for several reasons. Firstly, in those studies the tube array is subject to a cross flow of water for most tests, and so the relative magnitude of the fluid forces is much larger than is found for air (or gas) flow. Secondly, no account is taken of the inertial force ($m_s\ddot{y}$) of the structure in the parameter estimation procedure of these studies. This is permissible when the fluid forces are significantly larger than the inertial force as will be the case in water flow but not in air flow. Finally, and perhaps most importantly, in both those studies the behaviour of a fully flexible array was considered, and so the dominant mechanism for fluidelastic instability is likely to be stiffness controlled. Indeed, the fluid damping, which is of primary importance in this study, is not even considered as a separate parameter in the analysis of Tanaka and Takahara (1981), but rather is included as the imaginary part of a complex fluid force coefficient, which implicitly assumes a linear relationship between the fluid force and the tube motion. In the work of Chen et al. (1994) the linear fluid damping has been estimated directly, but the values obtained will be very sensitive to the phase characteristics of the instrumentation. For these reasons, an inverse method of parameter identification was chosen.

Only single degree of freedom oscillation in the lift direction is considered for a single flexible tube in an otherwise rigid array, which may not be indicative of a fully flexible array. Furthermore, as has been shown previously by Austermann and Popp (1995), the behaviour of the tube array may also depend on the position of the flexible tube. Therefore, the specific results obtained here may not be generally applicable to all normal tube arrays. However, the techniques described offer a method for more thorough validation of theoretical models than is possible simply by comparing limit cycle amplitudes and provide a framework for experimental investigation of the nonlinear behaviour of the coupled fluid–structure system.

2. Experimental facility

The tests were carried out in a down draught wind tunnel (test section dimensions of 300 mm × 300 mm × 750 mm) with a velocity range from 2 to 20 m/s and a free-stream turbulence level of less than 1%. An array of 38 mm diameter cylinders arranged in a normal triangular pattern, was placed in the test section as shown in Fig. 1. Two arrays with pitch ratio (P/d) of 1.32 and 1.58 were tested.

The tubes of each array were rigidly supported, except for one in the third row (shaded in Fig. 1) which although rigid, was supported at one end by a flexible mount consisting of two aluminium beams (3 mm × 50 mm × 500 mm) set parallel to each other 80 mm apart outside the wind tunnel. A sketch of the mounting scheme can be seen in Fig. 2. The advantage of this arrangement is that all motion is effectively suppressed except translation in the direction perpendicular to the flow. In contrast, a simpler cantilever support (commonly used in these types of experiments in the past) would permit pitching of the tube, while supporting the tube at both ends introduces a hardening spring effect. Pitching of the tube on the current setup is possible, but this involves higher modes of vibration as the rotational stiffness of the tube mount is large when compared to a cantilever support.

A series of random force response tests were conducted in quiescent air at several levels of excitation to ensure that the structure was dynamically linear, to locate the modes of the structure and identify the structural modal parameters. The natural frequency of the first structural mode was at 6.6 Hz, while that of the next mode was above 70 Hz. These tests demonstrated that the system behaves as a linear single degree of freedom system in the frequency range of interest.

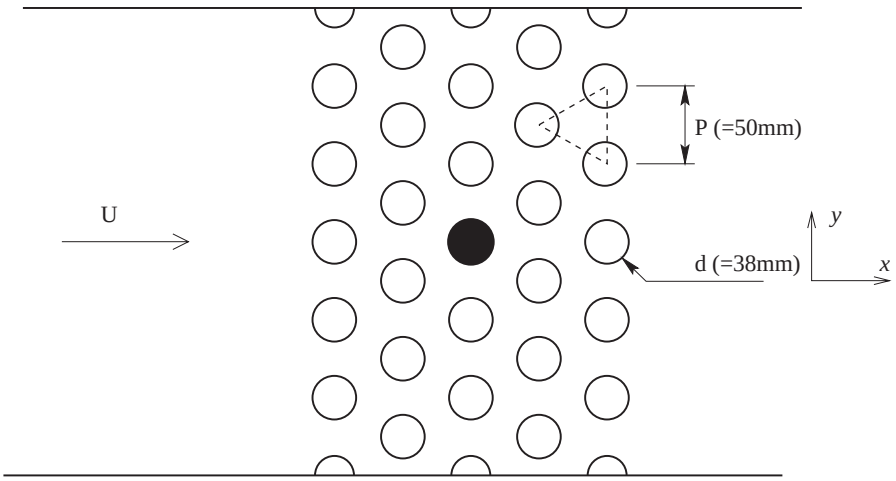

Fig. 1. Schematic of cross flow system.

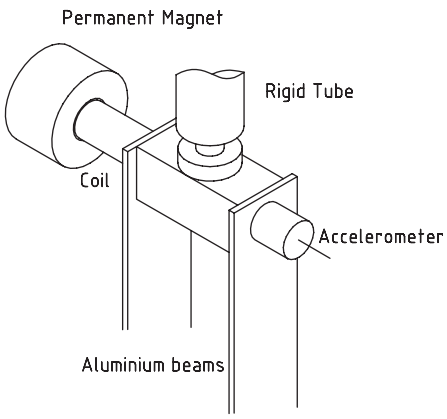

Fig. 2. Flexible tube detail.

A novel feature of the rig was a custom built electromagnetic shaker (referred to below as the EMS) which allowed the tube to be excited with an additional force. The shaker consists of a permanent magnet with an annular gap between the poles through which a copper coil wound around a cylinder of resin-impregnated paper may move. The magnet is fixed to the wind tunnel while the coil is attached to the tube support. In contrast to commercially available devices, there is no structural connection between the coil and the magnet so the apparent structural stiffness is not modified. Once the coil is part of an electrical circuit, the EMS introduces additional damping to the system. The level of damping can be chosen by changing the total electrical resistance in the circuit. This method of adjusting the damping is similar in principle to that used by Andjelic and Popp (1989), but has the advantage of being passive, so that the EMS can be used as a passive damping device and as an excitation source simultaneously. It can be shown that the additional damping force will be inversely proportional to the resistance of the circuit:

$$c_{em} = \frac{G_{em}}{R}, \tag{1}$$

where c_{em} is the additional electromagnetic damping, G_{em} is a constant which depends on the geometry and magnet flux density of the EMS, and R is the circuit resistance. It has been found that the variation of the apparent total structural damping with circuit resistance follows the theoretical trend very well. Furthermore, the natural frequency is unaffected so that damping can be modified independently of the stiffness or mass.

Tube acceleration was measured using a piezoceramic (charge) accelerometer with a useful frequency range of 0.2–3500 Hz (based on a maximum 5% variation in sensitivity). The accelerometer was mounted on the tube support as shown (Fig. 2). A laser vibrometer was focused on the accelerometer to provide a direct measure of the instantaneous velocity. The performance of the laser vibrometer is defined by an envelop bounded by a minimum amplitude of vibration of 10 nm, a maximum velocity of 2 m/s and a maximum frequency of vibration of 10 kHz. The sensitivity is constant from DC to the maximum frequency. Tube displacement was monitored with a noncontact capacitive displacement transducer which can measure vibration up to 5 kHz with an accuracy of 0.04% of the full-scale deflection. The readings from these instruments were digitized and logged using an 8 channel, 13-bit, synchronous data acquisition frame. Each channel had an independent progammeable gain amplifier and autoranging facility to ensure that at least 12 bits per channel were used in each data acquisition so as to minimize quantization error.

3. Fluidelastic thresholds

A series of tests were conducted to investigate the stability thresholds of the two array geometries with the one degree of freedom tube located in the third row. At each flow velocity the tube was released from rest and then allowed 300 s to establish a steady motion. The resistance in the EMS circuit was varied to obtain three different levels of damping for each array so that the instability thresholds lay within the wind tunnel velocity range.

Figs. 3 and 4 show the r.m.s. of the tube displacement for array pitch ratios of 1.58 and 1.32, respectively. The rapid increase in vibration amplitude characteristic of fluidelastic instability is apparent and it is obvious that the value of damping determines the flow velocity at which this occurs. This is the instability threshold or critical velocity, U_c and it was found in both arrays to be independent of whether the flow velocity was increasing or decreasing (i.e., there was no evidence of hysteresis).

An abrupt drop in amplitude at around 9 m/s can be seen in Fig. 4 for the pitch ratio of 1.32. Unlike the critical velocity, this drop does not depend on damping. A loud acoustic resonance was clearly audible at this velocity and the frequency (determined with a microphone outside the windtunnel, downstream of the array) was found to be 1053 Hz. Unfortunately the limit of the wind tunnel velocity range with this array was 9 m/s so it was impossible to explore the behaviour of the array at higher velocities and so verify that the instability would in fact re-establish itself after the conditions for acoustic resonance had been exceeded. A similar effect was reported by Price and Zahn (1991) and their observations indicated that the interaction between the acoustics and the structural dynamics could augment instability as well as suppressing it.

Based on a width of 300 mm the second transverse acoustic mode of the duct would be 1130 Hz. However, as the wind tunnel walls are slightly compliant, a figure of 1053 Hz is not unreasonable. No such resonance was observed for the pitch ratio of 1.58, suggesting that the resonance is particular to this array, rather than to the wind tunnel. Fig. 5 shows the tube-free response spetcra for the range of flow velocities. The power spectra, in decibels, have been scaled and offset for clarity. A peak (denoted by ◦) whose frequency depends on flow velocity indicates excitation by vortex shedding with a Strouhal number of 2.2 based on free-stream flow velocity. This figure is consistent with results of both Polak and Weaver (1995) and Oengoren and Ziada (1998). At 9 m/s this Strouhal number yields a shedding frequency of 522 Hz, which is close to half the acoustic resonance frequency. It might have been expected that the vortex shedding

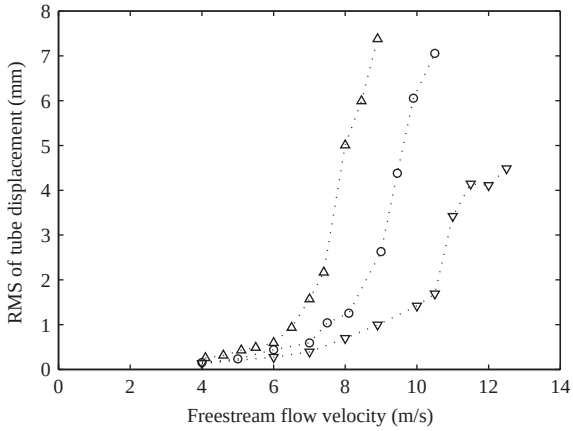

Fig. 3. R.m.s. of tube motion. $P/d = 1.58$ at three levels of damping: Δ, $\delta = 0.015$; $\circ$, $\delta = 0.023$; ∇, $\delta = 0.031$.

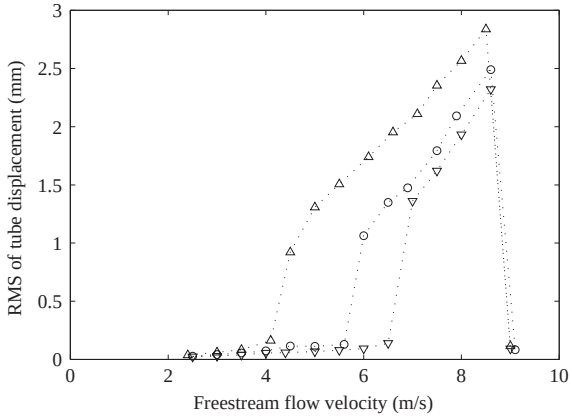

Fig. 4. R.m.s. of tube motion. $P/d = 1.32$ at three levels of damping: Δ, $\delta = 0.093$; $\circ$, $\delta = 0.106$; ∇, $\delta = 0.114$.

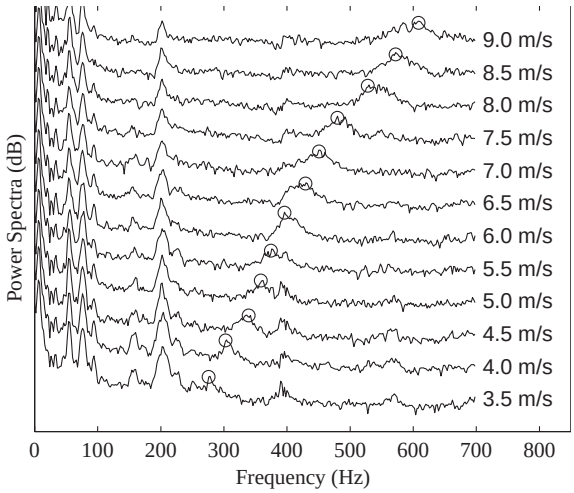

Fig. 5. Power spectra of tube acceleration; $P/d = 1.32$. Vortex shedding peak denoted with $\circ$.

Table 1
FEI thresholds

Pitch ratio (P/d)	1.58	1.58	1.58	1.32	1.32	1.32
Logarithmic decrement, δ	0.015	0.023	0.031	0.093	0.106	0.114
Critical velocity, U_c (m/s)	7.1	8.5	10.3	4.1	5.5	6.5
Reduced velocity, $U_c/(f_n d)$	28.1	33.6	40.8	16.2	21.8	25.7
Reduced gap velocity, V_r	33.9	40.5	49.1	57.3	77.1	90.8

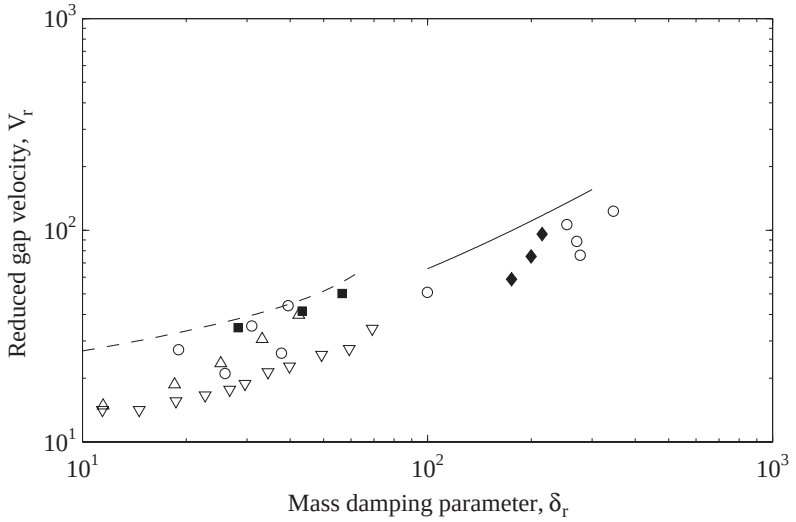

Fig. 6. Comparison of measured stability threshold: ∇, Austermann and Popp (1995), $P/d = 1.25$; Δ, Austermann and Popp (1995), $P/d = 1.375$; ◦, Price and Zahn (1991), $P/d = 1.375$; ▩, present, $P/d = 1.58$; ◆, present, $P/d = 1.32$; - - -, linear model, $P/d = 1.58$; —, linear model, $P/d = 1.32$.

would excite the first acoustic mode, however, Oengoren and Ziada (1998) note that under certain circumstances the first acoustic mode is completely suppressed. Additional work is needed to investigate the interaction of vortex shedding, acoustic resonance and tube vibration, however, further analysis is beyond the scope of the current study.

The critical velocities obtained from Figs. 3 and 4 are shown in Table 1. The reduced velocity is simply the nondimensionalized critical velocity. The reduced *gap* velocity, which was proposed by Chen (1984) in an attempt to collapse data from different array geometries and pitch ratios, is defined as

$$V_r = \left(\frac{P}{P-d}\right)\left(\frac{U}{fd}\right)\left(\frac{1}{2.105(P/d-0.9)}\right). \tag{2}$$

The stability threshold in terms of the reduced gap velocity is shown in Fig. 6 together with data from Austermann and Popp (1995) and Price and Zahn (1991). These two sources are by no means the only data available, but they have a similar set-up (normal triangular array with a single flexible cylinder in air). As can be seen, the current results compare favourably with the data available from these studies indicating that the experimental facility is typical of other reported rigs.

The simplest evidence of nonlinearity in the coupled flow–structure system can be seen in the variation of limit cycle amplitude with flow velocity (Figs. 3 and 4). Since the structure is linear, the fact that the tube exhibits a finite limit cycle amplitude, rather than simply a dynamic divergence, indicates that there must be a nonlinear relationship between tube motion and the fluid force. However, the presence of these nonlinearities may not be significant in tube motions at lower amplitude. In order to assess whether a full nonlinear model is necessary, linearized fluid force parameters have been examined.

4. Linearized fluid force model

Granger (1990) has estimated the linear stiffness, damping and mass associated with the fluid force directly from turbulent buffeting. That study was, in effect, examining small perturbations from the equilibrium position. The parameters obtained gave excellent predictions for the FEI threshold and the vibration amplitude before the onset of instability. The quality of the model predictions is indicative of the fact that the onset of FEI, which is an unstable perturbation, is governed by the linearized parameters for small motions about the equilibrium.

In this study, the linearized parameters have been obtained from large amplitude vibrations (i.e., motion not in the vicinity of the equilibrium) and then used to predict the stability thresholds (Fig. 6). Comparison between these predictions and the experimentally determined values offers an indication of the applicability of a nonlinear fluid force model.

A series of transient tests in which the flexible tube was given an initial displacement of 11 mm and released from rest were conducted for a range of flow velocities and levels of structural damping. The data acquisition was triggered by the tube velocity so that it was possible to perform an ensemble average in the time domain. For each condition (fluid velocity and structural damping) 10 records, each with 4 s of data at a sampling rate of 2048 Hz were obtained and averaged.

4.1. Identification technique

The equation of motion for the tube under fluid loading is

$$m_s\ddot{y}_i + c_s\dot{y}_i + k_s y_i = E(y_i, \dot{y}_i, \ddot{y}_i) + T_i(t), \tag{3}$$

where y_i is the displacement of the tube in test i, c_s is the system damping in quiescent air, k_s is the system stiffness in quiescent air, $E(y, \dot{y}, \ddot{y}_i)$ is the fluidelastic force, $T_i(t)$ is the turbulent excitation in test i.

Assume that the response can be decomposed into the sum of the response to the fluidelastic excitation and the random turbulent excitation,

$$y_i(t) = y_E(t) + y_T(t), \tag{4}$$

where $y_E(t)$ and $y_T(t)$ are defined by

$$m_s\ddot{y}_E + c_s\dot{y}_E + k_s y_E = E(y_E, \dot{y}_E, \ddot{y}_E), \tag{5}$$

$$m_s\ddot{y}_T + c_s\dot{y}_T + k_s y_T = T(t). \tag{6}$$

This assumes there is no interaction between the excitation mechanisms (i.e., the right-hand side of Eqs. (5) and (6) are linearly independent). Strictly speaking this is not valid, since the fluidelastic excitation depends on tube motion which will in turn be influenced by the turbulent excitation. However, if the tube motion is large, this interaction will be small. If n tests are conducted with the same initial conditions, one would expect $y_E(t)$ to be identical for each test. The turbulent response y_T however will vary randomly from one test to the next, so as $n \to \infty$, $\sum y_T(t) \to 0$. Thus if the ensemble is averaged, only the fluidelastic response will be left

$$y(t) = \frac{1}{n}\sum_{i=1}^{n} y_i(t) \approx \frac{1}{n}\sum_{i=1}^{n} y_E(t). \tag{7}$$

The equation of motion associated with the ensemble average response is

$$m_s\ddot{y} + c_s\dot{y} + k_s y = E(y, \dot{y}, \ddot{y}). \tag{8}$$

It has been widely assumed that if the vibration amplitude is small, this force can be represented as a second order differential operator (e.g., Granger, 1990)

$$E(y, \dot{y}, \ddot{y}) = -m_f\ddot{y} - c_f\dot{y} - k_f y, \tag{9}$$

where the subscript f denotes the fluid dynamic parameters.

Since the fluid in this study is air, the added fluid mass, m_f, is negligible, so that the linearized equation of motion for the system becomes

$$m_s\ddot{y} + (c_s + c_f)\dot{y} + (k_s + k_f)y = 0. \tag{10}$$

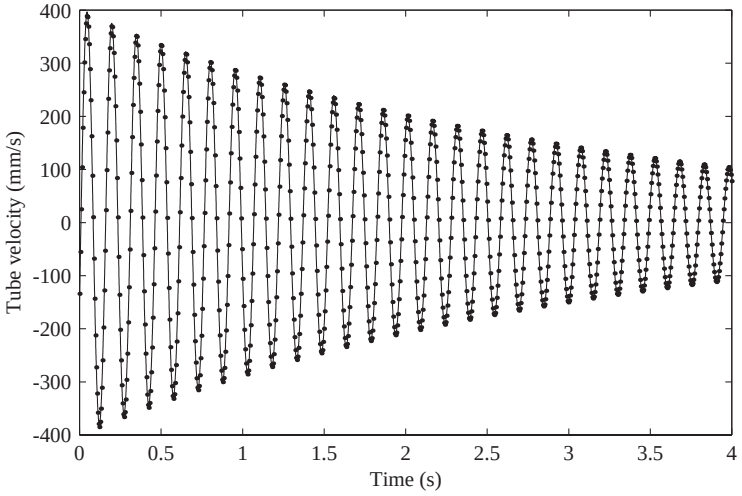

Fig. 7. Typical fit of Eq. (11), $P/d = 1.58$, $U = 9$ m/s. –, Experimental data; •, fitted curve.

The transient velocity response of Eq. (10) is

$$\dot{y}_{fit} = \alpha_1 e^{-\alpha_2 t} \sin(\alpha_3 t + \alpha_4) + \alpha_5, \tag{11}$$

where α_1, α_4 are arbitrary constants, $\alpha_2 = (c_s + c_f)/(2m_s) = \zeta\omega$, $\alpha_3 = \omega \approx \sqrt{(k_s + k_f)/(m_s)}$, α_5 is the mean value.

Although a nonzero mean tube velocity is unrealistic, it is permitted here to account for any DC bias introduced by the instrumentation.

The experimental transient response can now be fitted to the exponentially decaying sinusoid given by Eq. (11). This is achieved by using the downhill simplex search (Nelder and Mead, 1965) to minimize the objective function

$$\varepsilon = \sum_{t=0}^{4s} |\dot{y}(t) - \dot{y}_{fit}(t)|, \tag{12}$$

with the five parameters, α_i, $i = 1 \ldots 5$ as variables. An example of a curve fit obtained in this way can be seen in Fig. 7. The fitted curve has been decimated in the plot for clarity.

Once estimates of these parameters have been obtained the fluid damping and stiffness coefficients can be recovered easily since the modal parameters of the structure are known.

4.2. Linearized fluid force parameters

Linearized fluid force parameters have been obtained for both arrays ($P/d = 1.58$ and 1.32), with the flexible tube in the third row at various levels of structural damping. The equivalent linear damping coefficient, c_f, associated with the fluid force is shown in Figs. 8 and 9 for pitch ratio of 1.58 and 1.32, respectively. The coefficients are negative, indicating that the fluid is imparting energy to the structure, rather than dissipating it. Initially, at low flow velocity, there is some evidence to suggest that the net damping in the 1.58 array is increased by the fluid loading. This is supported by Granger (1990) who measured a fluid damping 6 times larger than the structural damping at low velocities, but that study was in water. This increase is caused by the fluid dynamic drag which occurs even in quiescent fluid. The magnitude of this drag force increases quadratically with the flow velocity while the direction of the drag force rotates from the transverse direction at zero flow to close to the inline direction when $\dot{y} \ll U$. At intermediate velocities, the destabilizing components of the fluid elastic force begin to dominate and the fluid damping decreases almost linearly with flow velocity.

The fluid stiffness has been extracted from the raw parameter estimates, although it is not as critical as the fluid damping for this type of fluidelastic instability. The fluid stiffness for each array is plotted in Figs. 10 and 11. Interestingly, the data for $P/d = 1.58$ follows closely a quadratic variation with flow velocity, suggesting a dependence on the flow dynamic head. This is not true for $P/d = 1.32$ where the trend seems to be closer to linear.

It is worth noting that over the entire flow velocity range considered the fluidelastic frequency (i.e., the frequency of vibration under fluid loading) varies by less that $\frac{1}{4}$ Hz for $P/d = 1.58$ and less than $\frac{1}{2}$ Hz for $P/d = 1.32$. Had a

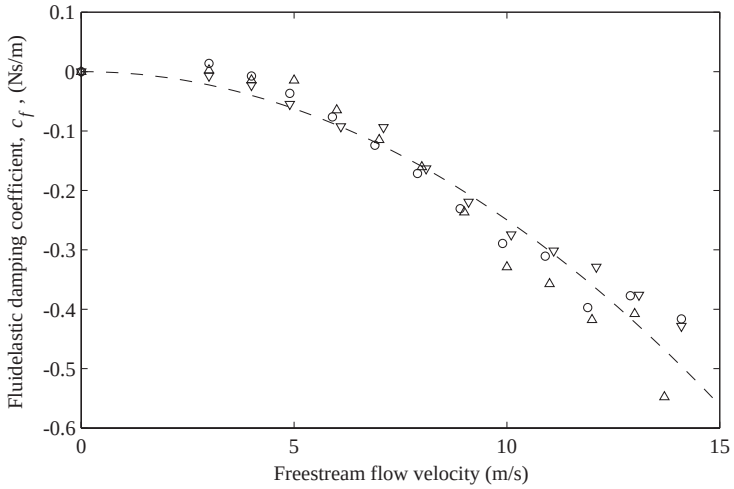

Fig. 8. Linearized fluid damping, c_f, for $P/d = 1.58$: Δ, $\delta = 0.15$; $\circ$, $\delta = 0.10$; ∇, $\delta = 0.05$; ---, quadratic fit.

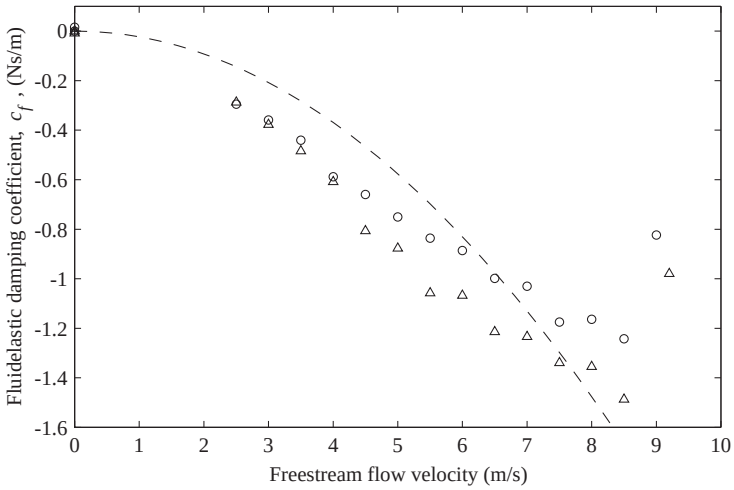

Fig. 9. Linearized fluid damping, c_f, for $P/d = 1.32$: Δ, $\delta = 0.19$; $\circ$, $\delta = 0.16$; ---, quadratic fit.

frequency domain analysis been employed, the effect of fluidelastic stiffness on the frequency would have been masked as the maximum frequency resolution for this data is $\frac{1}{4}$ Hz.

The effect of the acoustic resonance is clearly visible in both fluid damping and stiffness. In Figs. 9 and 11 the magnitude of the fluid force parameters drops sharply in the region of $U = 9$ m/s.

In general there is less scatter in the fluid stiffness data than the damping, but this can be attributed to the fact that the fluid damping force is nearly an order of magnitude smaller than the fluid stiffness force.

In order to facilitate the use the damping data to predict the stability thresholds, a third order polynomial was fitted to each data set subject to the constraint that it passes through the origin. This is a physical constraint, since there can be no fluid force when there is no flow.

4.3. Predictions

The variation of fluid force parameters with flow velocity can now be used in a simple linearized model of the fluid–structure dynamics to predict the instability threshold. The fluid stiffness is always positive, which means that a static divergence is impossible in this velocity range. Furthermore, a linearized stiffness must, by definition, be conservative. Therefore, the fluid stiffness can be ignored when estimating the critical velocity.

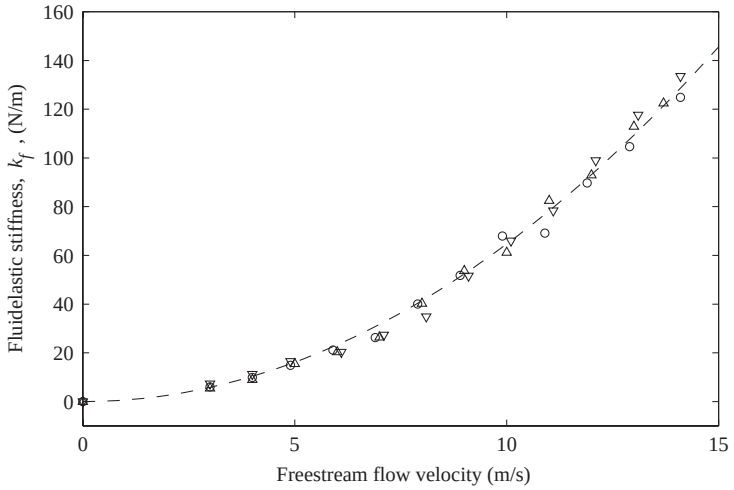

Fig. 10. Linearized fluid stiffness, k_f, for $P/d = 1.58$: Δ,$\delta = 0.15$; $\circ$, $\delta = 0.10$; ∇, $\delta = 0.05$; ---, quadratic fit.

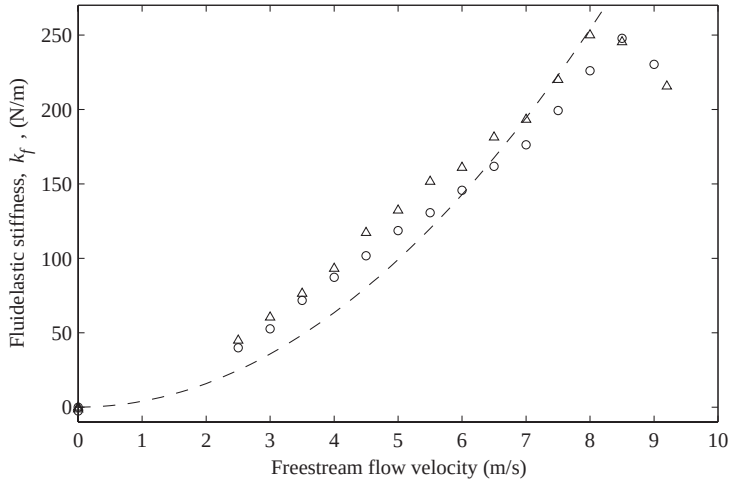

Fig. 11. Linearized fluid stiffness, k_f, for $P/d = 1.32$: Δ, $\delta = 0.19$; $\circ$, $\delta = 0.16$; ---, quadratic fit.

For a linearized model, instability is caused by a dynamic divergence. This means that the tube motion will be oscillatory, but with increasing amplitude of vibration. A limit cycle is not possible, except at the stability threshold which occurs when the fluid damping exactly counteracts the dissipation within the structure

$$c_s = -c_f. \tag{13}$$

Combining this condition with the empirically determined expressions describing the variation of c_f with flow velocity obtained from Figs. 8 and 9, a prediction for the stability boundary for each array is obtained. These stability boundaries are plotted in Fig. 6. The extent of the error in the predictions can be assessed from Table 2.

The predictions for a pitch ratio of 1.58 systematically overestimate the experimentally determined values of critical velocity by about 20%. It might have been expected that the predictions would have been closer, since the fluid force coefficients were measured experimentally. However, in light of the low contribution of the damping force to the total force (about 1%) this level of error is acceptable, particularly when compared to the theoretical predictions of Rzentkowski and Lever (1998) which indicate a critical velocity twice that observed here. It is true that other researchers (e.g., Tanaka and Takahara, 1981; Granger, 1990) have obtained closer agreement between linear models with

Table 2
Predictions for FEI thresholds using a linearized model

Pitch ratio	1.58	1.58	1.58	1.32	1.32	1.32
Logarithmic decrement, δ	0.015	0.023	0.031	0.093	0.106	0.114
Mass damping parameter, δ_r	28.2	43.3	58.42	175.3	199.8	214.8
Reduced gap velocity, V_r	33.9	40.5	49.1	57.3	77.1	90.8
Predicted reduced gap velocity	38.2	47.7	60.1	104.9	120.3	127.3
% Error	12.7	17.8	22.4	83.1	56.0	40.2

experimentally determined parameters and the experimental stability thresholds, but these studies have been conducted in water, and so the magnitude of the fluid forces was more significant.

The situation is considerably worse for a pitch ratio of 1.32. At the lowest level of mass damping parameter the critical velocity from the linear model is nearly 100% in excess of the actual value observed, improving to an error of 40% at the highest level of damping considered. This large error cannot be attributed simply to systematic experimental error as the contribution of fluid damping forces is about 4 times more significant than in the other array. It is likely that the assumption of linearity itself is responsible for the large discrepancy in the predictions. Since the fluid force is inherently nonlinear, any effective linear parameter estimate will include some contribution from nonlinear components. These results suggest that for large amplitude vibrations, a linearized model is acceptable for a pitch ratio of 1.58 but is not appropriate for the more densely packed array.

4.4. Forced response

In order to further demonstrate that nonlinearities are stronger for a pitch ratio of 1.32, a series of forced response tests under fluid loading have been conducted. The tube was excited by the EMS with a band-limited (2–40 Hz) periodic chirp, with a 16 s period. The amplitude of excitation was set at three levels, with the maximum chosen so as to avoid impacting between the tube and the wind tunnel wall. Typical transfer functions between acceleration and excitation force for the three levels of excitation are shown in Figs. 12 and 13, corresponding to a pitch ratio of 1.58 and 1.32, respectively.

The transfer function for pitch ratio of 1.58 does exhibit some amplitude dependence. The resonant peak value drops by about 20% (from 22.5 ms^{-2}/N at low excitation to 18.5 ms^{-2}/N at high excitation). The second array also shows a dependence on the excitation amplitude, but here it is more apparent. The effective damping clearly increases with excitation level (a reduction in FRF peak value) while the fluidelastic frequency decreases, implying nonlinear elements in both fluid stiffness and damping. Since the more closely packed array exhibits more significant nonlinear behaviour, the discussion will focus solely on the array with a pitch ratio of 1.32.

Based on the observations in this section, the general behaviour of a nonlinear model of the fluid force can be summarized in Table 3.

5. Nonlinear fluid force model

Rearranging Eq. (8) and recalling that the fluid added mass is negligible yields

$$m_s\ddot{y} = (E(y, \dot{y}, U) - c_s\dot{y} - k_s y). \tag{14}$$

The fluid elastic force can be decomposed into three functions, one in tube displacement y, the second containing only coupled terms and the third in tube velocity $\dot{y}$

$$E(y, \dot{y}, U) = -N_1(y, U) - N_2(y, \dot{y}, U) - N_3(\dot{y}, U). \tag{15}$$

The minus signs are included for consistency with the linear structural stiffness and damping. In the absence of any additional excitation force, the instantaneous force acting on the tube is simply the product of the mass and the acceleration. It should be noted that the linear model of the fluidelastic force considered previously in Section 4 is simply the special case where it is assumed that $N_2 = 0$ and that N_1,N_3 are linear. The same free response data which was used to obtain linearized parameter estimates are used here to obtain nonlinear parameter estimates.

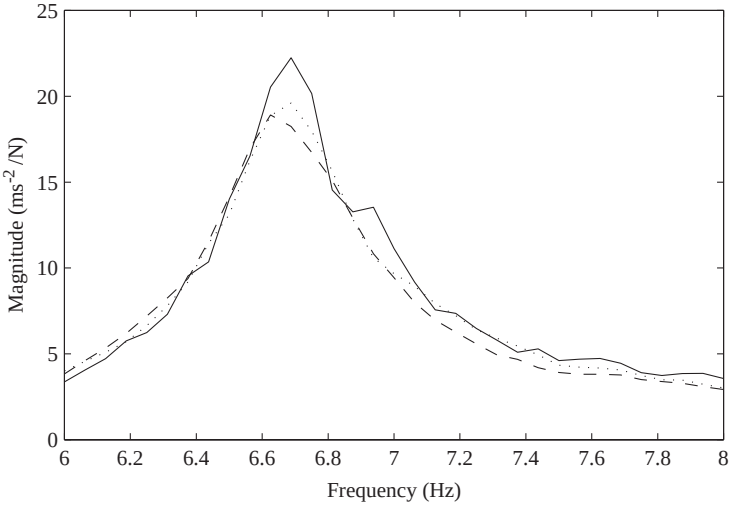

Fig. 12. FRF with fluid loading at three different levels of excitation, $U = 12$ m/s, $P/d = 1.58$: —, low excitation; ···, intermediate excitation; - - -, high excitation.

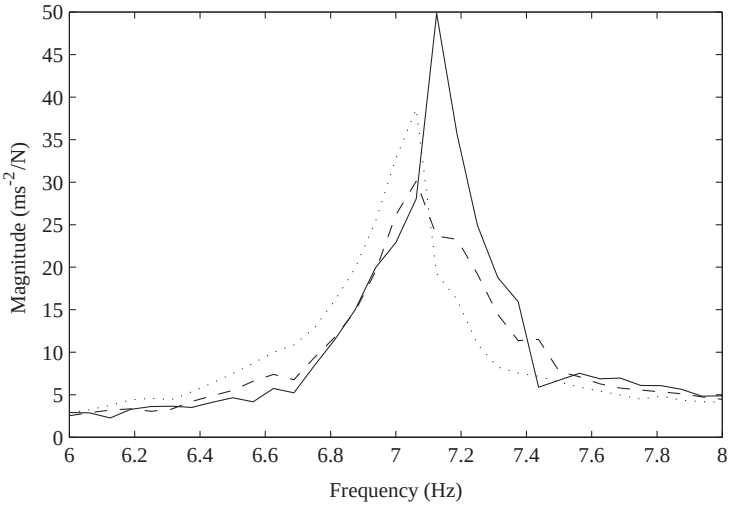

Fig. 13. FRF with fluid loading at three different levels of excitation, $U = 8$ m/s, $P/d = 1.32$: —, low excitation; ···, intermediate excitation; - - -, high excitation.

Table 3
Qualitative behaviour of a nonlinear model

	Increased flow velocity	Increased response amplitude
Total effective damping	Decreases	Increases
Total effective stiffness	Increases	Decreases

Combining Eqs. (14) and (15) yields an expression for the restoring force F which accounts for the effect of both the structure and the fluidelastic force:

$$m\ddot{y} = F(y, \dot{y}, U) = -(N_1(y, U) + k_s y) - N_2(y, \dot{y}, U) - (N_3(\dot{y}, U) + c_s \dot{y}). \tag{16}$$

As the modal mass of the structure m_s is known (1.05 kg), the instantaneous restoring force is also known. To obtain a model for the fluid force for each freestream flow rate, the total force may be approximated by a surface above the

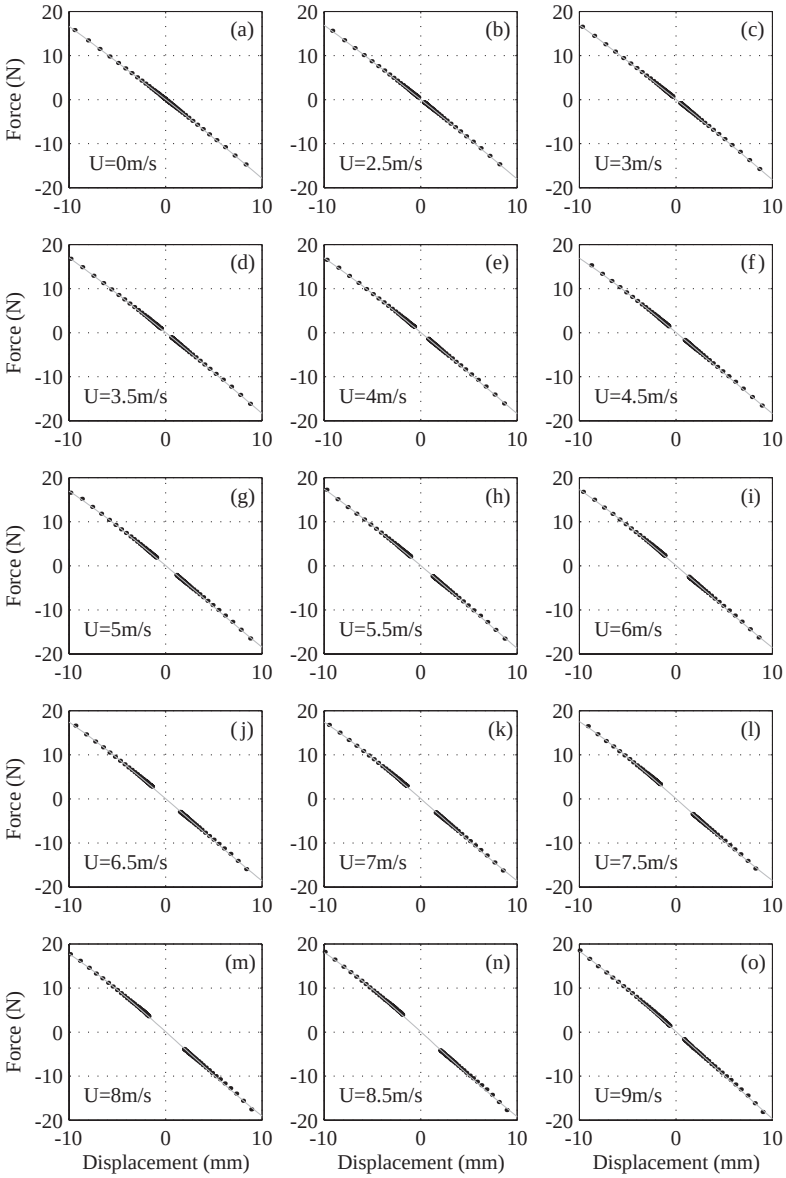

Fig. 14. Total stiffness force against tube displacement.

state plane $(y, \dot{y})$. This approach to nonlinear system identification, referred to as the force state mapping technique, was first proposed by Masri and Caughey (1979) and several applications of the method can be found in the literature (Masri et al., 1987; Worden, 1990; Xu and Rice, 1998). Additional details of the application of the force state mapping technique to this system can be found in Meskell et al. (2001).

In order to explore the functional form of N_1 and N_3, and hence F, the intersection of the force state map with the zero tube displacement and tube velocity planes has been calculated and are shown for a range of flow velocities in Figs. 14 and 15, respectively. It should be noted that in Fig. 14 $N_2 = N_3 = 0$ as $\dot{y} = 0$ while in Fig. 15 $N_1 = N_2 = 0$ since $y = 0$. Thus,

$$F_{y=0} = -(N_3(\dot{y}) + c_s\dot{y}), \tag{17a}$$

$$F_{\dot{y}=0} = -(N_1(y) + k_s y). \tag{17b}$$

The relatively high data density at lower displacement amplitudes in Fig. 14 is due to the motion decaying exponentially. As the amplitude approaches zero, the rate of change of amplitude is slower, and so the decrease in the zero

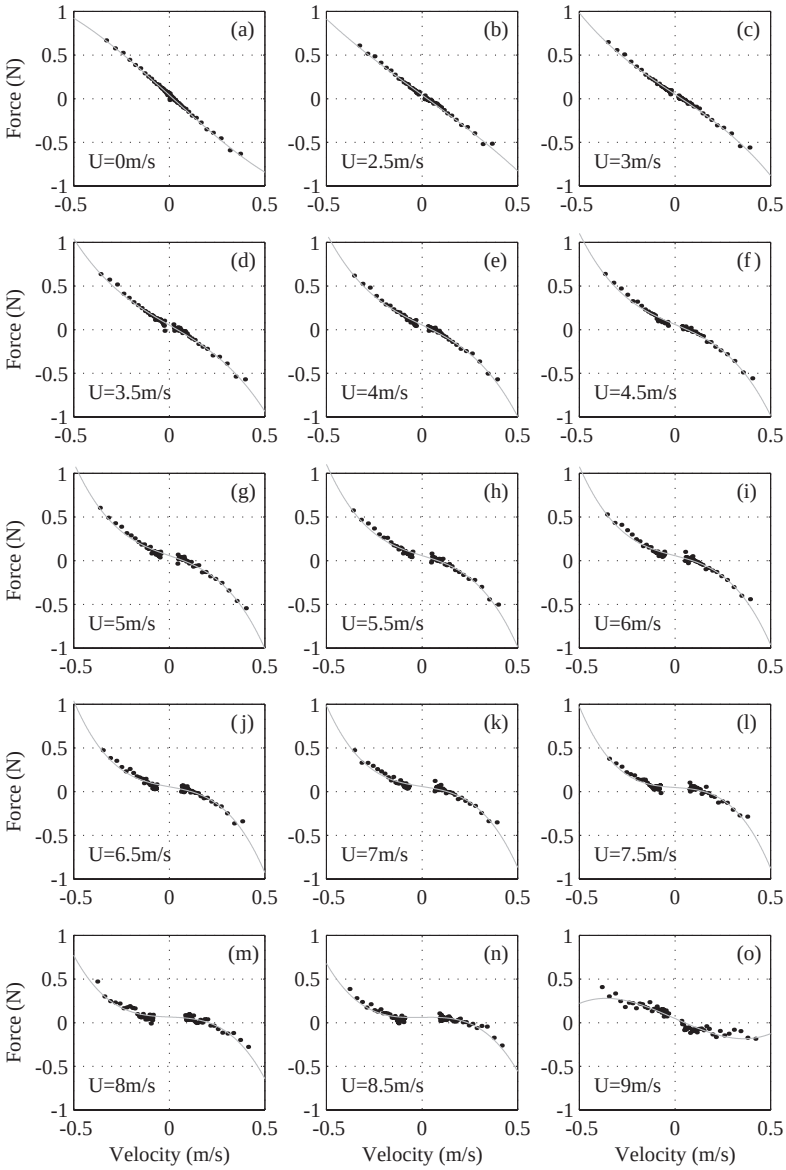

Fig. 15. Total damping force against tube displacement.

velocity displacement from one period to the next is much smaller at the end of the decay than at the start. The same is true for Fig. 15.

There appears to be more scatter in the data of Fig. 15 than is evident for the displacement–force data (Fig. 14). This can be attributed to two mechanisms.

The velocity measurement was monitored using 12-bit ADC, just as the displacement was, so one would expect a comparable signal-to-noise ratio. The acceleration is a subset of the same measurement as that used in Fig. 14, but the range of acceleration in the zero displacement plane is more than a factor of 30 smaller than the full range of measurement. This means that the force data is more susceptible to noise in the acceleration record. Furthermore, although the raw acceleration data was digitized with 12-bit precision, the force data in Fig. 15 will have only 7-bit precision ($2^{12}/30 \approx 2^7 = 128$ levels) so quantization error may be an issue. The intersection between the force surface and the zero displacement plane is calculated by interpolating between the two points measured as the state-space trajectory crosses the plane. This will mask the stratification of data which is characteristic of quantization error, but will not alleviate it.

To illustrate the second mechanism, consider the tube motion to be a fixed amplitude sine wave. When the velocity crosses zero, both the displacement and the acceleration are changing slowly with time (both are at the peak/valley of the sine wave). This means that if the time at which the velocity is zero is miscalculated due to noise in the velocity record, neither the corresponding displacement nor force will be strongly affected. The situation at the displacement zero crossing is not the same. Here, the acceleration is changing rapidly, so noise in the displacement record may produce a large error in estimating the force at zero displacement. Thus, the displacement–force curves (Fig. 14) are not susceptible to noise in the tube velocity, but the velocity–force (Fig. 15) curves may be corrupted by errors in the displacement record.

Notwithstanding the scatter in the data, there is a clear trend, which is flow velocity dependent, in the graphs of Fig. 15. In order to emphasize the nonlinearity of these trends, a straight line has been fitted to the each data set and then subtracted, thus removing the dominant linear relationship between velocity and force. The resulting residuals are shown in Fig. 16. It is apparent that these residuals are not random, but are in fact governed by a predominantly

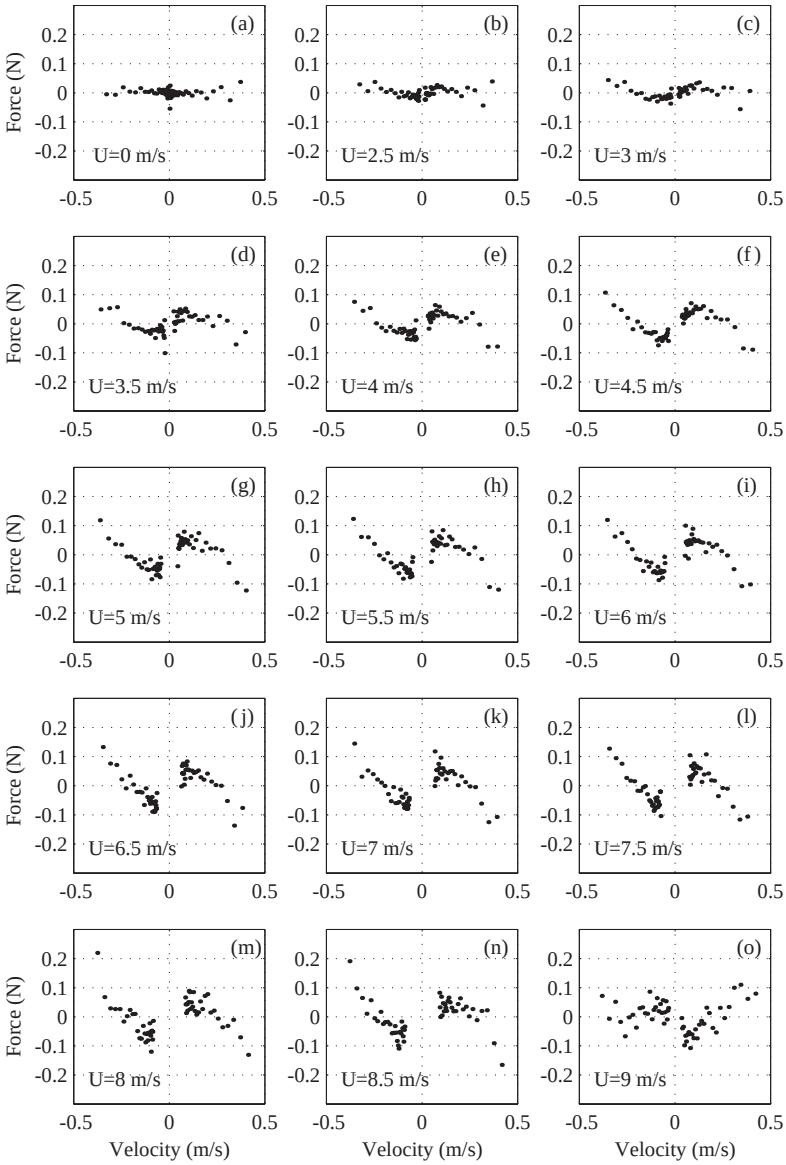

Fig. 16. Velocity–force data with the linear trend removed.

antisymmetric function, which becomes more pronounced with increased flow velocity. Similar, though less pronounced behaviour was also noted for the data of Fig. 14.

Therefore, it was assumed that the fluidelastic force can be represented as the sum of a cubic stiffness and a cubic damping. This model is perhaps the simplest which will satisfy the qualitative observations of the behaviour. It also has the advantage that the fluid force has only antisymmetric (odd) terms which would be expected due to geometric symmetry of the tube array,

$$N_1 = \eta y^3 + k_f y, \tag{18}$$

$$N_2 = 0, \tag{19}$$

$$N_3 = \beta \dot{y}^3 + c_f \dot{y}, \tag{20}$$

$$\Rightarrow F = -(\eta y^3 + (k_s + c_f)y) - (\beta \dot{y}^3 + (c_s + c_f)\dot{y}). \tag{21}$$

Thus the intersection of the force surface with the zero velocity (Fig. 14) and zero displacement (Fig. 15) planes will yield

$$F_{y=0} = -\beta \dot{y}^3 - (c_s + c_f)\dot{y}, \tag{22a}$$

$$F_{\dot{y}=0} = -\eta y^3 - (k_s + k_f)y. \tag{22b}$$

The model is similar to that developed by Price and Valerio (1990). The main difference is that in their model, the fluid stiffness exhibits very strong nonlinearity, which results in relatively large amplitude harmonics in the free response of the tube. This phenomenon has not been observed here. Notwithstanding that, the basic mechanism which limits the tube motion is high order (i.e., greater than 1) polynomial terms in the fluid damping. Price and Valerio also allowed for cross terms in their formulation (i.e., $N_2 \neq 0$). In this study, once the parameters of Eq. (21) had been estimated (see below), the time series of cross term N_2 was calculated for each flow velocity:

$$N_2(t) = m\ddot{y} - [N_1(y(t)) + k_s y(t) + N_3(\dot{y}(t)) + c_s \dot{y}(y)]. \tag{23}$$

Unfortunately, no functional relationship between N_2 and $(y, \dot{y})$ was apparent. The only trend to emerge was that the r.m.s. of N_2 increased with flow velocity from almost zero at no flow to 0.3 N at 8.5 m/s. This does not imply that there is no cross term at work in the fluid structure system, only that it is immersed in noise. However, without a model for the functional form, N_2 must be ignored. As will be discussed later, this represents the main weakness of this study.

5.1. Results

Eqs. Eq. (22) have been fitted to each data set in Figs. 14 and 15. A total least-squares estimator was used since errors are equally likely to occur in the measured force ($\ddot{y}$) as in the state variable measurement ($\dot{y}$ or y). The fitted curves are superimposed on the data for comparison.

Since the structural stiffness k_s and damping c_s are known, the fluidelastic model parameters, β, η, c_f and k_f can be estimated directly from the parameters obtained by the curve fit. The results of this parameter estimation are shown in Figs. 17–20. In Figs. 17 and 18 the variation of the linear and the cubic fluid stiffness can be seen, respectively, while Figs. 19 and 20 show the variation of the linear and the cubic fluid damping.

The positive linear fluid stiffness, indicating a total stiffness increasing with flow velocity, is consistent with the experimental observation of a frequency of oscillation which also increases with flow velocity. Although the nonlinear stiffness term does not play a significant role in the dynamics of this system, the negative sign of this parameter (η) is consistent with the qualitative observation of the system behaviour in Table 3. As will be demonstrated below, the fluid damping parameters are also consistent with the qualitative behaviour of the experimental system.

In order to simplify the prediction of the system behaviour based on this model, the variation of the parameters with velocity can be represented as low order polynomials in the range $U = 2.5 \rightarrow 8.5$ m/s. The order of the polynomial is arbitrary and chosen by inspection

$$\begin{aligned} k_f &= B_1 U + A_1, \\ \eta &= B_2 U + A_2, \\ c_f &= B_3 U + A_3, \\ \beta &= D_4 U^3 + C_4 U^2 + B_4 U + A_4. \end{aligned} \tag{24}$$

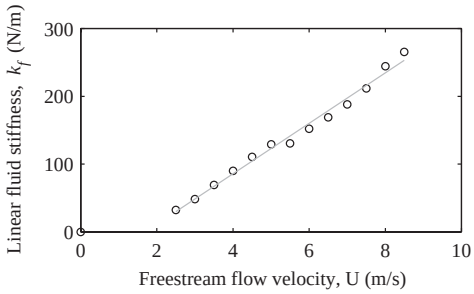

Fig. 17. Linear fluid stiffness coefficient.

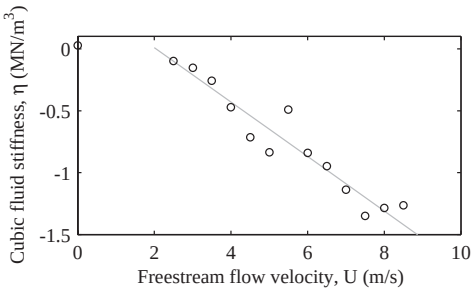

Fig. 18. Cubic fluid stiffness coefficient.

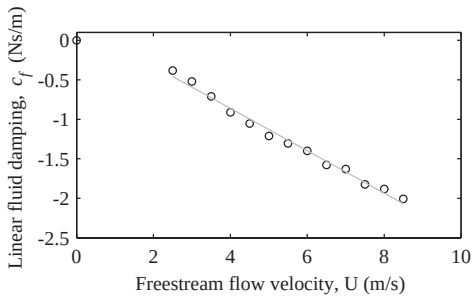

Fig. 19. Linear fluid damping coefficient.

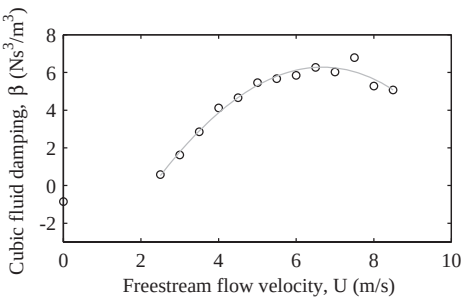

Fig. 20. Cubic fluid damping coefficient.

Table 4
Specific parameter values for the current array

	A	B	C	D
k_f	−40	29	—	—
η	0.45	−0.22	—	—
c_f	0.21	−0.27	—	—
β	−7.83	3.99	−0.245	-5.4×10^{-3}

The specific values of the coefficients are obtained by simple regression of the data in Figs. 17–20. These values are summarized in Table 4.

5.2. Behaviour of the empirical nonlinear model

There are three aspects of the behaviour of the model which are of immediate interest: the fluidelastic threshold, the limit cycle amplitude and the stability of the limit cycle.

The work done by the coupled fluid–structure system during a single period of oscillation is given by

$$W = \int_0^{2\pi/\omega} F(y,\dot{y},U)\,\dot{y}\,\mathrm{d}t \tag{25}$$

where ω is the circular frequency of vibration and F is the total force (structural and fluidelastic) acting on the tube (see Eq. (16)).

The convention that negative work indicates energy being dissipated from the structure has been adopted. The total force as a function of tube displacement and velocity has been determined empirically above

$$F(y,\dot{y},U) = -[(k_f(U)+k_s)y + \eta(U)y^3 + (c_f(U)+c_s)\dot{y} + \beta\dot{y}^3]. \tag{26}$$

Substituting Eq. (26) into Eq. (25) yields the work done per cycle in terms of the model parameters:

$$W = -\int_0^{2\pi/\omega} [(k_f+k_s)y + \eta y^3 + (c_f+c_s)\dot{y} + \beta\dot{y}^3]\,\dot{y}\,\mathrm{d}t. \tag{27}$$

Since $(k_f+k_s)y$ and ηy^3 are conservative forces, they will do no work over one period and the expression can be further reduced

$$W = -\int_0^{2\pi/\omega} (c_f+c_s)\dot{y}^2\,\mathrm{d}t + \int_0^{2\pi/\omega} \beta\dot{y}^4\,\mathrm{d}t. \tag{28}$$

Assume that over one cycle the tube displacement is given by a constant amplitude sinusoid.

$$y = A\sin(\omega t),$$
$$\Rightarrow \dot{y} = -A\omega\cos(\omega t). \tag{29}$$

A constant amplitude is admissible since the damping levels (whether positive or negative) are low so that the amplitude of vibration is changing slowly. Considering the motion to have only a single frequency component, rather than a combination of harmonics, is justified by the weakness of the nonlinearities.

Using Eq. (29) in Eq. (28)

$$W = -A^2\omega^2(c_f+c_s)\int_0^{2\pi/\omega} \cos^2(\omega t)\,\mathrm{d}t + A^4\omega^4\beta\int_0^{2\pi/\omega} \cos^4(\omega t)\,\mathrm{d}t, \tag{30}$$

$$\Leftrightarrow W = -A^2\omega\pi\left[(c_f+c_s) + \frac{3}{4}(\beta A^2\omega^2)\right]. \tag{31}$$

It should be noted that ω, c_f and β are functions of the flow velocity U, which have been determined empirically in the last section.

When the tube motion has established a limit cycle, the total work done during the course of one cycle period must be zero,

$$\Rightarrow W = 0. \tag{32}$$

Combining this condition with Eq. (31) provides an expression for the limit cycle amplitude in terms of the parameters from the cubic damping model. Some manipulation yields

$$\Leftrightarrow A = \sqrt{-\frac{4}{3}\frac{(c_f(U) + c_s)}{\beta(U)\,\omega(U)^2}}. \tag{33}$$

Since β is positive in the range of interest (Fig. 20), and ω by definition is positive (a negative frequency in this situation implies a static divergence), the limit cycle amplitude predicted by Eq. (33) will be real only if $(c_f + c_s)$ is negative. At first, this appears to be the same criterion as was used to obtain stability threshold predictions from the linearized model. However, since the effect of the nonlinear damping (which for the cubic model has a stabilizing influence) is accounted for explicitly rather than by measuring an apparent linear damping, the estimates of c_f from the nonlinear model are substantially different from those of the linearized model. This can be seen by comparing Fig. 9 with Fig. 19.

If the limit cycle is to be stable, any perturbation to the limit cycle must decay. In other words, if the motion is disturbed so that the amplitude of motion is increased, the work done per cycle must be negative to dissipate the added energy. Conversely, a reduction in the vibration amplitude must produce positive net work, so that energy is transferred from the flow into the structure. Therefore, $\partial W/\partial A$ must be negative. Differentiation of Eq. (31) yields

$$\frac{\partial W}{\partial A} = -A\pi\omega[2(c_f + c_s) + A^2 3\beta\omega^2]. \tag{34}$$

Substituting the limit cycle amplitude obtained from Eq. (33) into the equation above yields a simplified expression for the derivative at the limit cycle amplitude,

$$\left(\frac{\partial W}{\partial A}\right)_{LC} = 2\pi\omega A(c_f + c_s). \tag{35}$$

As the limit cycle amplitude A is nonzero and $2\pi\omega$ is positive, $\partial W/\partial A$ will be negative only if $(c_f + c_s)$ is negative. This is the same condition for the nonlinear model to yield a real valued limit cycle amplitude that was noted above. Therefore, any limit cycle amplitude predicted by the model will be stable. It has been suggested by Rzentkowski and Lever (1992, 1998), that the cause of the hysteretic behaviour of the fluidelastic stability threshold can be attributed to the possibility of an unstable limit cycle. In this context, the fact that the cubic damping model identified here predicts that any limit cycle which occurs will be stable is supported by the observation made in Section 2 that neither array under investigation exhibited hysteretic behaviour.

5.3. Predictions

Using parameter estimates from Eq. (24) in Eq. (33) the variation with flow velocity of r.m.s. of the tube response was calculated for the same three damping conditions as were used in the tests of Section 2. These predictions can be seen in Fig. 21. The critical velocities predicted by the nonlinear model are more accurate than those from the linear model, as can be seen in Table 5.

Comparing Fig. 4 with Fig. 21 clearly shows that the predicted limit cycle amplitudes for post stable behaviour are of the order of 100% greater than those observed experimentally. Nonetheless, there is good qualitative agreement between experimental results and the identified nonlinear model.

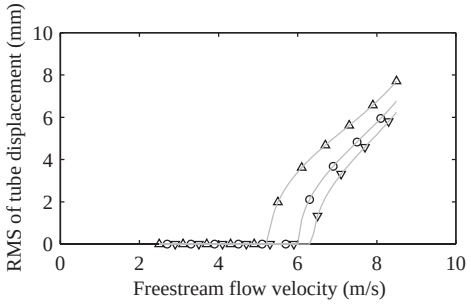

Fig. 21. Predicted r.m.s. tube displacement: Δ, $\delta = 0.093$; ◦, $\delta = 0.106$; ∇, $\delta = 0.114$.

Table 5
Predictions for FEI thresholds using a nonlinear model

Pitch ratio	1.32	1.32	1.32
Logarithmic decrement, δ	0.093	0.106	0.114
Reduced gap velocity, V_r (Fig. 4)	57.3	77.1	90.8
Linearized model	104.9	120.3	127.3
Nonlinear model (Fig. 21)	72.6	83.8	88.0
% Error in linearized model (Table 2)	83.1	56.0	40.2
% Error in nonlinear model	26.7	8.7	3.2

There are several possible explanations for the discrepancies between the observed and predicted amplitudes. The most obvious is that potential cross terms (i.e., terms involving a cross product of y and $\dot{y}$) in the fluid force model were neglected. Such terms would couple tube displacement and velocity, and would reasonably be expected to contribute to the dynamics of the system. No effort has been made to include turbulent buffeting in the predictions of tube motion. While this is valid for the parameter identification procedure, it is not appropriate for predicting response amplitude. Rzentkowski and Lever (1998) have shown that turbulent buffeting (or indeed any random excitation uncorrelated with the tube motion) would decrease the observed amplitude of vibration by as much as 25%.

The cubic damping parameter, β, is responsible for stabilizing the system and so an underestimation of this parameter would lead to an over estimation of the limit cycle amplitude. It is worth noting that the r.m.s. of the cubic fluid damping force is less than 0.5% of the overall system restoring force F, so some error in parameter estimation is likely. The parameter estimates obtained with the force state mapping technique are very sensitive to phase errors in the response data (see Meskell and Fitzpatrick, 2002). Combining the functional forms determined by force state mapping from this study with a parameter identification procedure which is more robust to phase errors may produce better estimates of the limit cycle amplitude. Such a scheme was proposed by Mottershead and Stanway (1986) and extended to systems with weak nonlinear damping by Meskell (2000). However, further work, either theoretical or experimental is needed to determine the appropriate functional form for the cross term N_2.

6. Conclusions

Two normal triangular tube arrays with a single flexible tube have been tested subject to cross flow at large amplitudes of vibration. Linearized fluid force parameters have been identified from free response data using a nonlinear curve fitting technique. It has been found that for a pitch ratio of 1.58 the critical velocities based on these parameters compared well with experimentally determined thresholds. However, in the array with pitch ratio of 1.32, the predicted instability thresholds did not agree well with experimental results, indicating that nonlinearity between fluid force and the tube motion is more significant in more closely packed arrays. Further direct evidence of the extent of nonlinear behaviour has been obtained by considering the forced response of the tube under fluid loading at different levels of excitation (i.e., displacement). It was found that for a pitch ratio of 1.58 the FRF was not modified significantly, implying a pseudo-linear system is adequate for modelling purposes. For the denser array however, the damping clearly increased with amplitude and there was a slight shift in natural frequency indicating a decrease in total stiffness.

An empirical nonlinear model has been proposed for the fluid force the parameters of which have been obtained from free decay data using the force state mapping technique. The nonlinear model was then used to predict critical velocity for instability and the subsequent post-stable behaviour. Comparison of the results with experimental data showed good agreement for the critical velocity prediction. Although similar trends for the limit cycle amplitudes have been obtained, the values are systematically over-predicted and several possible sources of this error have been identified. Nonetheless, direct evidence of nonlinearity in the coupled fluid–structure system has been presented and a qualitative assessment of the behaviour has been made.

References

Andjelic, M., Popp, K., 1989. Stability effects in a normal triangular cylinder array. Journal of Fluids and Structures 3, 165–185.

Austermann, R., Popp, K., 1995. Stability behaviour of a single flexible cylinder in rigid tube arrays of different geometry subject to cross-flow. Journal of Fluids and Structures 9, 303–322.

Chen, S., 1984. Guidelines for the instability flow velocity of tube arrays in crossflow. Journal of Sound and Vibration 93, 439–455.
Chen, S., Zhu, S., Jendrzejczyk, J., 1994. Fluid damping and fluid stiffness of a tube row in crossflow. ASME Journal of Pressure Vessel Technology 116, 370–383.
Granger, S., 1990. A new signal processing method for investigating fluidelastic phenomena. Journal of Fluids and Structures 4, 73–97.
Masri, S.F., Caughey, T.K., 1979. A non-parametric identification technique for nonlinear dynamic problems. Journal of Applied Mechanics 46, 433–447.
Masri, S.F., Miller, R., Saud, A., Caughey, T.K., 1987. Identification of non-linear vibrating structures. Part i: formulation. Part ii: applications. Journal of Applied Mechanics 54, 918–929.
Meskell, C., 2000. A parameter identification procedure for systems with weak non-linear damping forces. In: Sas, P., Moens, D. (Eds.), ISMA25 Noise and Vibration Engineering, Vol. 2, Katholoeke Universiteit Leuven, Leuven, pp. 679–686.
Meskell, C., Fitzpatrick, J.A., 2002. Errors in parameter estimates from the force state mapping technique for free response due to phase distortion. Journal of Sound and Vibration 252, 967–974.
Meskell, C., Fitzpatrick, J.A., Rice, H.J., 2001. Application of force-state mapping to a nonlinear fluid-elastic system. Mechanical Systems and Signal Processing 15, 75–85.
Mottershead, J., Stanway, R., 1986. Identification of *n*th-power velocity damping. Journal of Sound and Vibration 105, 309–319.
Nelder, J., Mead, R., 1965. A simplex method for function minimization. The Computer Journal 7, 308–313.
Oengoren, A., Ziada, S., 1998. An in-depth study of vortex shedding, acoustic resonance and turbulent buffeting in normal triangular tube arrays. Journal of Fluids and Structures 12, 717–758.
Paidoussis, M., 1979. Flow-induced vibrations in nuclear reactors and heat exchangers (practical experiences and state of knowledge). In: Naudascher, E., Rockwell, D. (Eds.), Practical Experiences with Flow-Induced Vibration. Springer, Berlin, pp. 1–81.
Paidoussis, M., Li, G., 1992. Cross-flow-induced chaotic vibrations of heat-exchanger tubes impacting on loose supports. Journal of Sound and Vibration 152, 305–326.
Polak, D.R., Weaver, D., 1995. Vortex shedding in normal triangular tube arrays. Journal of Fluids and Structures 9, 1–18.
Price, S.J., 1995. A review of theoretical models for fluidelastic instability of cylinder arrays in cross-flow. Journal of Fluids and Structures 9, 463–518.
Price, S.J., Valerio, N., 1990. A nonlinear investigation of single degree of freedom instability in cylinder arrays subject to cross flows. Journal of Sound and Vibration 137, 419–432.
Price, S.J., Zahn, M.L., 1991. Fluidelastic behaviour of a normal triangular array of subject to cross-flow. Journal of Fluids and Structures 5, 259–278.
Rzentkowski, G., Lever, J., 1992. Modeling the nonlinear fluidelastic behaviour of a tube bundle. In: Paidoussis, M.P., Chen, S.S., Steininger, D.A. (Eds.), Cross Flow Induced Vibration of Cylinder Arrays. ASME, New York, pp. 89–106.
Rzentkowski, G., Lever, J., 1998. An effect of turbulence on fluidelastic instability in tube bundles: a nonlinear analysis. Journal of Fluids and Structures 12, 561–590.
Tanaka, H., Takahara, S., 1981. Fluidelastic vibration of tube arrays in cross flow. Journal of Sound and Vibration 77, 19–37.
Weaver, D., Fitzpatrick, J., 1988. A review of cross-flow induced vibrations in heat exchanger tube arrays. Journal of Fluids and Structures 2, 73–93.
Worden, K., 1990. Data processing and experiment design for the restoring force surface method. Part 1: integration and differentiation of measured time data. Part 2: choice of excitation signal. Mechanical Systems and Signal Processing 4, 295–344.
Xu, K.Q., Rice, H.J., 1998. On an innovative method of modeling general nonlinear mechanical systems. Part 1: theory and numerical simulations. Part 2: experiments. ASME Journal of Vibration and Acoustics 120, 125–137.